

Dark Matter searches using gravitational wave bar detectors: quark nuggets and newtorites

M. Bassan^{b,c,*}, E. Coccia^{b,f}, S. D'Antonio^c, V. Fafone^{b,c}, G. Giordano^a,
A. Marini^a, Y. Minenkov^c, I. Modena^b, G.V. Pallottino^d, G. Pizzella^a,
A. Rocchi^c, F. Ronga^{a,*}, M. Visco^{e,1}

^a*Istituto Nazionale di Fisica Nucleare - Laboratori Nazionali di Frascati,
Via E. Fermi, 40 - 00044 Frascati, Italy*

^b*Dipartimento di Fisica, Università di Tor Vergata,
Via della Ricerca Scientifica, - 00133 Roma, Italy*

^c*Istituto Nazionale di Fisica Nucleare - Sezione Roma Tor Vergata,
Via della Ricerca Scientifica, - 00133 Roma, Italy*

^d*Dipartimento di Fisica, Sapienza Università di Roma and Istituto Nazionale di Fisica
Nucleare Sezione Roma 1 - piazzale Aldo Moro 2, - 00185 Roma, Italy*

^e*Istituto di Astrofisica e Planetologia Spaziali - INAF
Via del Fosso del Cavaliere 100, 00133 Roma, Italy*

^f*Gran Sasso Science Institute, INFN, Viale F. Crispi 7 - 67100 L'Aquila, Italy*

Abstract

Many experiments have searched for supersymmetric WIMP dark matter, with null results. This may suggest to look for more exotic possibilities, for example compact ultra-dense quark nuggets, widely discussed in literature with several different names. Nuclearites are an example of candidate compact objects with atomic size cross section. After a short discussion on nuclearites, the result of a nuclearite search with the gravitational wave bar detectors Nautilus and Explorer is reported. The geometrical acceptance of the bar detectors is $19.5 \text{ m}^2 \text{ sr}$, that is smaller than that of other detectors used for similar searches. However, the detection mechanism is completely different and is more straightforward than in other detectors. The experimental limits we obtain are of interest because, for nuclearites of mass less than 10^{-5} g , we find a flux smaller than that one predicted considering nuclearites as dark matter candidates. Particles with gravitational only interactions (newtorites) are another example. In this case the sensitivity is quite poor and a short discussion is reported on possible improvements.

Keywords: Gravitational Wave Detectors, Dark Matter, Nuclearites, Newtorites, MACROs

*Corresponding authors: ronga@lnf.infn.it; bassan@roma2.infn.it

1. Introduction

During the last decade a very large experimental and theoretical effort has been devoted to understand the problem of dark matter (DM). DM is necessary to explain the rotation of Galaxies and the measurements of the velocities of galaxies in clusters of galaxy. The presence of DM is also predicted by the standard Λ CDM cosmological model that requires a non relativistic $\Omega_m \sim 0.31$ matter component and a baryonic component $\Omega_b \sim 0.05$ [1]. Therefore the remaining fraction $\Omega_{DM} \sim 0.26$ should consist of some kind of weakly interacting matter different from the normal baryonic matter. The local DM density in our galactic halo is expected to be of the order of 0.3 GeV/cm^3 , and the DM speed should have values typical of galactic halos, around 270 km/s .

The leading dark matter candidates are supersymmetric thermal relics, a class of stable weakly-interacting massive particles (WIMPs) that arise in supersymmetric theories; however searches for supersymmetry at LHC and other accelerators have not found signals to date [2]. Likewise, direct detection experiments have yet to make any conclusive detection of conventional WIMPs [3]. The DAMA experiment has detected a seasonal modulation in the signal that could be due to the dark matter[4], but up to now no other experiment has confirmed this finding. A possible signature of WIMPS could be the detection of γ or neutrinos by WIMP - antiWIMP annihilation inside celestial bodies. This search, called indirect detection, also has given no convincing signature[2]. Other DM candidates include primordial black holes, monopoles, axions and sterile neutrinos.

Another scenario predicts that that DM particles could be much heavier than the few TeV mass reached by current experiments. The possible existence of super-heavy dark matter particles, sometimes called Wimpzillas, would have interesting phenomenological consequences, including a possible solution of the problem of cosmic rays observed above the GZK cutoff [5]. Many exotic names are used in the literature for such particles: Q-balls, mirror particles, CHArged Massive Particles, (CHAMPs), self interacting dark matter, cryptons, super-weakly interacting dark matter, brane world dark matter, heavy fourth generation neutrinos, “MACROs”, *etc.* (see the references listed in [6]). Even if strongly interacting, these objects could remain ‘dark’ due to their large mass-to-surface area ratio and correspondingly low number density required to explain the observed DM mass density. There are some recent cosmological indications in favor of strongly interacting dark matter [7, 8]. However there is no experimental evidence supporting this idea. Recent reviews are in Ref [9, 10] and [11].

Composite objects consisting of light quarks in a color superconducting phase have been suggested as super-heavy quark nuggets DM; in addition, super-heavy DM anti-quark nuggets could exist and could perhaps solve the matter-antimatter asymmetry [12]; the detection of such anti-quark nuggets by cosmic ray experiments is discussed in [13]. The energy loss predicted for super-heavy DM particles varies in different models, but it is likely that for masses of the order of grams or more such particles could be confused with meteors, since the

velocity, 270 km/s, is in the high-end tail of the meteor velocity distribution[14]. Many names have been proposed for those objects: Quark nuggets, CUDOs [15], MACROs[16, 10, 11].

Here, we will focus our attention mainly on one possible kind of very massive particle called “nuclearite” [17]. It is an example of a well defined particle, consisting of neutral matter with strange quarks among its constituents, and has

already been searched for by other experiment. Moreover the nuclearite results can be easily extended to a generic strongly interacting particle.

Nuggets of Strange Quark Matter (SQM), composed of approximately the same numbers of up, down and strange quarks could be the true ground state of quantum chromodynamics [18]. SQM nuggets could be stable for all baryon numbers in the range between ordinary heavy nuclei and neutron stars. They may have been produced in the early Universe. SQM should have a relatively small positive electric charge compared to that of heavy nuclei [17]. Macroscopic quark nuggets, neutralized by captured electrons, are called nuclearites. Otherwise, as in the case of small baryon numbers ($A \leq 10^6$), assumed to be quasi totally ionized, they will be called strangelets. There are several concerns about the SQM hypothesis; one was raised in 1999, when heavy-ion collisions between gold nuclei were produced at the Brookhaven National Laboratory (USA) and, more recently, before the LHC run with heavy ions: negative strangelets would attract a positive nucleus and could swallow it, in a sequence that could end with the digestion of the whole planet. Fortunately, however, theoretical considerations suggest that negative strangelets are unlikely to exist [19, 20].

Finally it is important to note that quite unlikely the DM would consist of only one particle with a single mass and interaction; therefore, experimental searches should look at different possibilities with a variety of techniques.

In this paper we will discuss particle detection using the thermo-acoustic effect (see below, sect.2.2), and in particular with gravitational waves (gw) cryogenic bar detectors, expanding and improving the preliminary results presented in ref.[21]. We will focus on the Nautilus and Explorer detectors, that our group operated for decades. We will then describe the analysis procedure and the selection criteria to identify candidates events, i.e. those signal, among those recorded by the detectors as “outliers”, that are compatible with an excitation produced by one of the exotic particles described above. Then, starting from the energy distributions of the candidates events we will present upper limits both specialized for nuclearites and for generic MACRO particles, vs. both mass and cross section, as suggested in [9] and [16].

In another scenario, DM only interacts gravitationally. In this case the excitation of a bar detector is due directly to the newtonian force. The detection mechanism is much more efficient, but signals are very small because the newtonian force is extremely weak. The limits on this kind of DM with Nautilus and Explorer and the possible improvements will be discussed in the last section.

2. Gravitational wave bar detectors used as particle detector

2.1. *Nautilus and Explorer*

The *gw* bar detector Nautilus[22] is located in Frascati (Italy) National Laboratories of INFN; it started operations around 1998. The current run has been continuously ongoing since 2003. The detector Explorer[23], similar to Nautilus, was located in CERN (Geneva-CH) and was operational from 1991 to June 2010.

Both detectors work on the same operating principles. Explorer and Nautilus consist of a large aluminium alloy cylinder (3 m long, 0.6 m diameter) suspended in vacuum by a cable around its central section and cooled to about 2 K by means of a superfluid helium bath. The *gw* excites the odd longitudinal modes of the cylindrical bar, producing an oscillation that is then mechanically amplified by an auxiliary mechanical resonator tuned to the same frequency which is bolted on one bar end face. This resonator is part of a capacitive electro-mechanical transducer that produces an electrical a.c. current that is proportional to the displacement between the secondary resonator and the bar end face. Such current is then amplified by means of a low-noise dcSQUID superconductive device.

Central suspension and vacuum are used to reduce seismic and acoustic noise, while cooling to 2K reduces the thermal Nyquist noise of the electromechanical resonators. Nautilus is also equipped with a dilution refrigerator that enables operations at 0.1 K, further reducing the thermal noise. However, after 2001 the refrigerator was kept idle, because its operation negatively affected the detector duty cycle.

The output of the SQUID amplifier is conditioned by band pass filtering and by an anti-aliasing low-pass filter, then sampled at 5 kHz and stored on disk. Sampling is triggered by a GPS-disciplined rubidium oscillator, also providing the time stamp for the acquired data. The data are processed off-line, applying adaptive frequency domain filters optimized for delta-like signals, i.e. very short (few ms) bursts. We first whiten the data, i.e. remove the effect of the detector transfer function. A filter matched to delta excitations is then applied to this stream. The filter is designed and optimized for delta-like signals, but it works equally well for a wider class of short bursts, like e.g. damped sinusoids with decay time less than 5 ms. The noise characteristics estimate is updated averaging the output over 10 minutes periods. Traditionally, in the antenna jargon, the noise energy is expressed in kelvin units ($1 \text{ K} = 1.38 \times 10^{-23} \text{ J}$). The typical filtered noise of data considered in this paper is between 1 and 5 mK.

2.2. *The Thermo-Acoustic Model*

The interaction of energetic charged particles with a normal mode of an extended elastic cylinder has been extensively studied over the years, both on the theoretical and on the experimental side[24].

According to the so called “thermo acoustic model” a particle crossing the bar produces longitudinal vibrations originated from the local thermal expansion due to the warming up due to the energy loss. In particular, the vibration amplitude linearly depends on the ratio of two thermo-physical parameters of

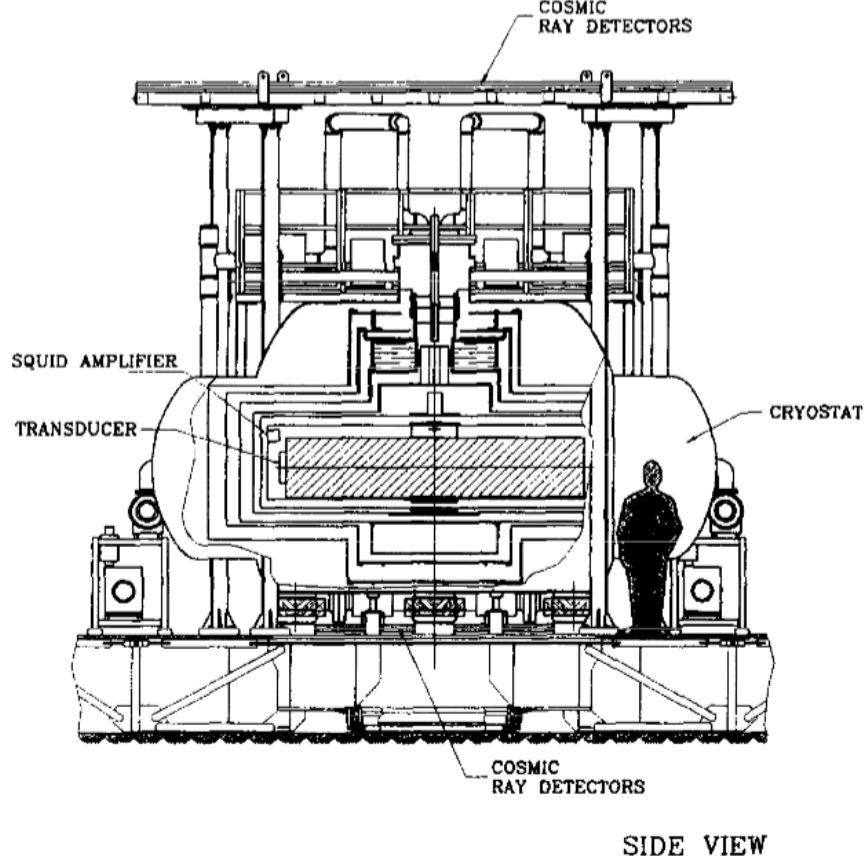


Figure 1: Schematic layout of the Nautilus *gw* bar detector.

the material, namely the thermal expansion coefficient and the specific heat at constant volume. The ratio of these two quantities appears in the definition of the Grüneisen parameter γ . It turns out that while the two thermo-physical parameters vary with temperature, γ practically does not, provided the temperature is above the material superconducting (*s*) state critical temperature.

The change in vibrational energy ΔE of the fundamental vibrational mode due the energy loss of a particle crossing an aluminium cylindrical bar is [25, 26, 27]:

$$\Delta E = \frac{4}{9\pi} \frac{\gamma^2}{\rho L v^2} \left(\frac{dW}{dx} \right)^2 \times \left[\sin\left(\frac{\pi z_o}{L}\right) \frac{\sin[(\pi l_o \cos(\theta_o)/2L)]}{\pi R \cos(\theta_o)/L} \right]^2 \quad (1)$$

where L is the bar length, R the bar radius, l_o the length of the particle track inside the bar, z_o the distance of the track mid point from one end of the

bar, θ_o the angle between the particle track and the axis of the bar, $\frac{dW}{dx}$ the energy loss of the particle in the bar, ρ the density, v the longitudinal sound velocity in the material. This relation is valid for the normal-conducting (n) state material and some authors (see the references in [24]) have extended the model to a super-conducting (s) resonator, according to a scenario in which the vibration amplitude is due to two pressure sources, one due to $s - n$ transitions in small regions centered around the interacting particle tracks and the other due to thermal effects in these regions now in the n state.

It is important to note, at this point, that a gw bar antenna, used as particle detector, has characteristics very different from the usual particle detectors which are sensitive to ionization losses: indeed an acoustic resonator can be seen as a zero threshold calorimeter, sensitive to a vast range of energy loss processes. The usual gw software filter works well up to a time scale of the order of 5 ms, corresponding to a $\beta = v/c = 4 \times 10^{-6}$ for a 60 cm particle track. So the antenna is sensitive to very slow tracks: this is another very important difference with respect to the usual particle detectors.

Due to this effect cosmic ray showers can excite sudden mechanical vibrations in a metallic cylinder at its resonance frequencies; in experiments searching for gw these disturbances are hardly distinguishable from the searched signal and represent an undesired source of accidental events, thus increasing the background. This effect was suggested many years ago and a first search was carried out with limited sensitivity on room temperature Weber type resonant bar detectors and ended with a null result [28]. To monitor these signals and to provide effective vetos, Nautilus was equipped with a cosmic ray shower telescope system, composed of streamer tubes detectors positioned both above and below the cryostat. For further details see ref.[29]. The first detection of cosmic ray signals in a gw antenna took place in 1998, with the Nautilus detector operating at a temperature $T = 0.14$ K [30], i.e. below the superconducting (s) transition critical temperature $T_c \simeq 0.9$ K. During this run, an unexpectedly large number of events with very large amplitude were detected. This result suggested an anomaly either in the thermo-acoustic model or in the cosmic ray interactions[31]. However the observation was not confirmed in the 2001 run with Nautilus at $T = 1.5$ K [29] and therefore we formulated the hypothesis that the unexpected behavior was due to the superconducting state of the material.

This result prompted the construction, in 2002, of a scintillator cosmic ray detector also for the Explorer gw detector [32] as well as the beginning of a dedicated experiment (RAP) [33, 34, 35], that was carried out at the INFN Frascati National Laboratory to study the vibration amplitude, caused by the hits of a 510 MeV electron beam, in a small Al5056 bar. The experiment was also motivated by the need of a better knowledge of the low temperature values of the thermo-physical parameters for the alloy Al5056, used in the bar detectors.

As a result of these experiments we have a model capable to predict the signal produced in a bar like that of Nautilus or Explorer by the interaction with a passing energetic particle:

for a particle that loses a total amount of energy W while intersecting the

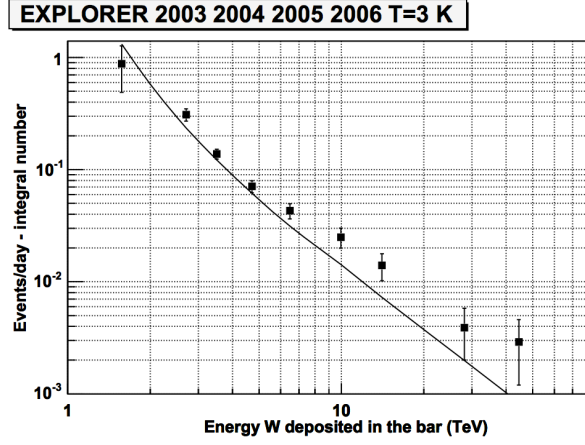


Figure 2: Integral distribution of extensive air showers in Explorer. The line shows the prediction based on the thermo acoustic model [32]. One event, the largest ever recorded, with an energy of 360 TeV. (670 K in kelvin units), sits at the far right outside this plot.

bar, orthogonally to its axis and through its middle section, the energy of the longitudinal fundamental mode of vibration will change by :

$$\Delta E \sim 7.64 \times 10^{-9} W^2 \delta_G^2 \quad [\text{K}] \quad (2)$$

where we assume negligible the bar oscillation energy before the interaction and we express ΔE in kelvin units and W in GeV units. The numerical constant has the value computed using the Grüneisen parameter γ of pure aluminium at 4 K. The parameter δ_G describes the correction due to different temperatures or materials:

the measurements, carried out on Al5056 alloy [24] , give: $\delta_{G,n} = 1.16$ for $T=4\text{K}$ and $\delta_{G,n} = 1.3$ for $T \sim 1.5$ K above the transition temperature ($T_c = 0.845\text{K}$), with a relative uncertainty of 6%. For superconductive Al5056 we found $\delta_{G,s} = 5.7 \pm 0.9$. Most of the events presented here were gathered with the antenna in equilibrium with a bath at $T \sim 1.5\text{-}2$ K.

Using the results of these measurements we have a good agreement both in rate and amplitude of the extensive ray shower detected in Nautilus and Explorer [32] as shown in fig.2, with the expectation based on cosmic ray physics and the thermo-acoustic model. This reinforces our confidence in a full understanding of the *gw* bar detectors used as particle detector.

3. Dark Matter signals in gravitational wave bars

3.1. MACROs and nuclearites

The interaction with the bar of massive candidates with radius R much larger than any microscopic length scale, e.g. the electron's Compton wavelength or the Bohr radius, is quite simple because we can ignore any quantum-mechanical

aspects of scattering, and any short-range interaction: the interaction cross-section σ corresponds then to the dark matter geometric cross-section. In ref [9] the name MACROs was proposed for this class of macroscopic dark matter. If the MACRO candidate carries a net charge, it may also interact electromagnetically. In this section we consider only neutral matter. Additional contribution to the energy lost by charged matter or antimatter will increase the expected signal.

The main energy loss mechanism for a generic neutral particle, having cross section σ , a non-relativistic velocity v and mass $M \gg M_{atomic}$, is by atomic collision:

$$\frac{dE}{dx} = -\sigma\rho v^2 \quad (3)$$

where ρ is the density of the traversed medium and v the particle velocity. In pure aluminium $\rho = 2700 \text{ kg/m}^3$. In the case of a compact object the cross section σ is the effective area A than can be computed via the compact object density ρ_N .

When a MACRO crosses the atmosphere (or the Earth), it loses energy and the velocity decreases according to:

$$v = v_0 e^{-\frac{\rho_a L \sigma}{M}} \quad (4)$$

where ρ_a is the atmosphere density, L is the path length, σ and M the particle cross section and mass. In order to be detectable in an analysis where delta like signals are selected, these excitations should be in the ms range and therefore the velocity v should be $\gtrsim 1 \text{ km/s}$.

Consider a MACRO of velocity $c\beta$, intersecting orthogonally through the center of the Nautilus (or Explorer) bar: by applying eq.2 we can compute the energy change ΔE of the bar fundamental mode (the “signal”):

$$\Delta E = 1.08 \cdot 10^{32} \left(\frac{\beta}{10^{-3}}\right)^4 \sigma^2 \quad [\text{K}] \quad (5)$$

Here σ is in cm^2 and we have used $\delta \sim 1.3$ at $T = 2\text{K}$ [24], and ΔE is measured in kelvin. So, an object having atomic size, as a nuclearite, produces signals in the 1 K region. Nuclearites with galactic velocities are protected by their surrounding electrons against direct interactions with the atoms they might hit. For a small nuclearite of mass less than 1.5 ng , the cross-section area A is controlled by its electronic atmosphere whose radius is never smaller than 10^{-8} cm :

$$A = \begin{cases} \pi \cdot 10^{-16} \text{ cm}^2 & \text{for } M < 1.5 \text{ ng} \\ \pi \left(\frac{3M}{4\pi\rho_N}\right)^{2/3} \text{ cm}^2 & \text{for } M > 1.5 \text{ ng} \end{cases} \quad (6)$$

where $\rho_N = 3.6 \cdot 10^{14} \text{ g/cm}^3$ is the nuclearite density and M its mass [17].

Consider indeed a nuclearite of mass M and velocity $c\beta$, intersecting orthogonally the center of the Nautilus (or Explorer) bar; by applying eq.5 we have:

$$\Delta E = 10.7 \left(\frac{\beta \theta(M)}{10^{-3}} \right)^4 \quad [\text{K}] \quad (7)$$

where ΔE is the energy variation of the bar fundamental mode measured in kelvin and $\theta(M) = (M/1.5 \text{ ng})^{1/3}$ if $M > 1.5 \text{ ng}$. Otherwise $\theta(M) = 1$.

The location of the detector used has impact on the range of σ and M that can be detected. For example according to eq.3, nuclearites having galactic velocity (about 300 km/s) and mass heavier than 10^{-14} g penetrate the atmosphere, while those heavier than 0.1 g pass freely through an Earth diameter.

3.2. Newtonites

Particles having newtonian interaction only can be called newtonites. Due to the long range nature of the newtonian force, signals could occur even if the particle does not cross the bar. In the case of a point like particle moving with a constant velocity v along a straight trajectory coming from infinity and going to infinity, the vibrational amplitude of the n th-vibrational mode is given by[26]:

$$A_n = -\frac{2GM}{Vv} \int_V \frac{\mathbf{u}_n \cdot (\mathbf{x}_T - \mathbf{x}_T^0)}{(x_T - x_T^0)^2} d^3\mathbf{x} \quad (8)$$

Here G is the gravitational constant, M the mass of the newtonite, \mathbf{x}_T are the transverse coordinates of a volume element of the detector relative to a fixed point \mathbf{x}_T^0 , arbitrarily chosen along the particle track; \mathbf{u}_n is the spatial part of the n th normal-mode oscillation normalized to the volume V of the bar. For a thin bar with radius r and length L , ($r \ll L$) \mathbf{u}_n can be approximately written, using cylindrical coordinates [27]:

$$\begin{aligned} u_n^r &= \sqrt{2}\sigma_P\pi(r/L)\sin(n\pi z/L) \\ u_n^z &= \sqrt{2}\cos(n\pi z/L) \end{aligned} \quad (9)$$

Here σ_P is the aluminium Poisson module. The energy variation in the bar is obtained by:

$$\Delta E_n = \frac{1}{2k_B} \rho A_n^2 V \quad [\text{K}] \quad (10)$$

Here k_B is the Boltzman constant. In this paper we are only interested in the first longitudinal mode $n=1$, and we assume that the velocity v of the particle is large enough that most of the signal is contained in a few ms. This requirement is due to the δ -like filter used to extract the antenna events. (different filters could in principle detect longer signals, lasting up $\sim 40\text{s}$). The signal is a fairly complicated function of the newtonite's trajectory and has been computed in [26] in the particular case of orthogonal trajectory in the middle of the bar, and for $r/L \rightarrow 0$. In this case we can put $u_1^r = 0$ and we obtain:

$$\Delta E \sim 30\pi r^2 \frac{\rho G^2}{k_B L} \left(\frac{M}{v} \right)^2 \quad [\text{K}] \quad (11)$$

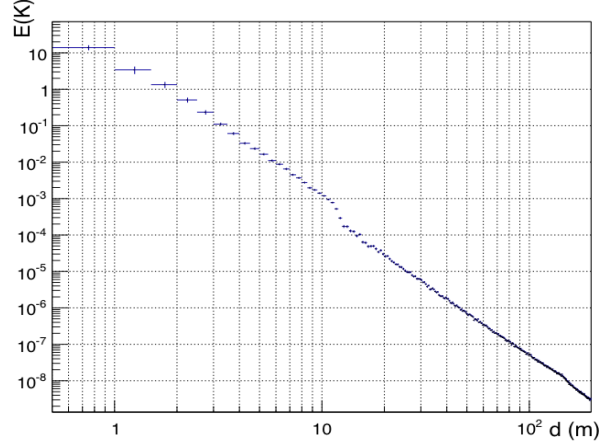


Figure 3: Average from different directions of the signals due to a $M/v = 10 \text{ kg s/km}$ newtorite vs. distance from the bar center

Numerically we have for Nautilus $\Delta E \sim 2.4(M/v)^2 \text{ K}$ with M expressed in kg and v in km/s.

In the general case the signal has been computed by numerical integration of eq.8 inserted in a Montecarlo to simulate random directions. The result of one of those calculations as function of the distance of the trajectory from the bar center and for $M/v=10 \text{ kg s/km}$ is shown in Fig 3. From this figure we can see that, at large distance d , the signal energy scales as $1/d^4$, as expected from eq.8. The signal falls below the energy threshold used in this analysis (see the next paragraphs) for d larger than $\sim 3 \text{ m}$ for $M/v=10 \text{ kg s/km}$. For $M/v=100 \text{ kg s/km}$ this threshold occurs at $d \gtrsim 10 \text{ m}$.

4. Data processing and selection

In this section we describe the procedure to select large signals that emerge, in a statistical sense, from the noise of the antenna. We shall call them candidate events or simply events, but this does not imply any assumption on their origin or cause. As mentioned in sect.2.1, for this analysis we considered the stream of delta-filtered data sampled at 5 kHz. Indeed, the signal expected from the interaction of a nuclearite with the bar has the characteristics of the response to a delta-like excitations, and we take advantage of this to reject events not compatible with a delta. In this respect, the search for this class of events is more demanding than the usual coincidence searches for g.w. candidates.

In the filtered data we search for *candidate events* by applying a threshold, usually set at 4 times the RMS value, continuously updated in an exponentially weighted manner. This produces a large number of events, a few thousands per day, with a gaussian amplitude distribution, but with a tail of high amplitude events consistently higher than for a gaussian. In the past, this behavior has been extensively studied and a number of possible causes for this instrumental

extra-noise was identified: seismic excitations, instabilities of the SQUID electronics, electrically induced spikes, shaking due to the cryogenic fluids, cosmic rays showers, and so on.

In this work, we have considered only the events with energy larger than 0.1 K . As the RMS noise is of the order of a few mK, the number of these large signals reduces from thousands to tens per day.

The data processing applied for the present work can be divided in two parts: first we select the periods of “good” operation and then we proceed with the identification of spurious events

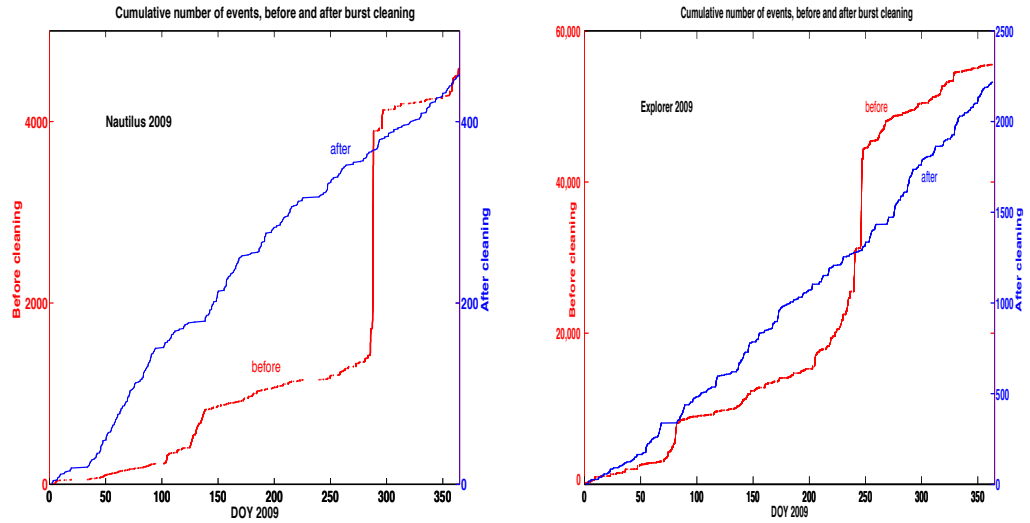


Figure 4: Cumulative time distribution of the Explorer and Nautilus events during year 2009. One can clearly see that there are periods with a rate of events orders of magnitude larger than in the quiet periods of operation. For each detector, we show the distribution before (red online) and after (blue online) the cuts operated to remove the noisy periods. The selections reduces the number of events by a factor between 10 and 20.

4.1. Selection of periods of operation

The first selection step is to remove the periods that were marked by operator’s flags or comments, indicating that maintenance operations were going on. Further cuts are performed by looking at the amplitude, in the unfiltered data, at the frequency of a reference tone that is added in the SQUID electronic for the purpose of monitoring the gain of the whole electronic chain. These two cuts usually reduces the livetime by $\simeq 20 - 30\%$

A third selection is based on the seismic noise as detected by some accelerometers mounted on the bars cryostat and recorded by an ADC sampled at 0.1024 Hz. When the seismic noise exceeds a previously set threshold, a period of at

least 10 s is vetoed. This cut removes a negligible amount of livetime, but several large events.

A fourth selection considers the value of the *effective temperature* T_{eff} , i.e., the variance of the filtered data, measured in K . As previously said, this value was usually around 1-2 mK for Nautilus and 2-3 mK for Explorer. We

vetoed periods of at least 10 minutes when T_{eff} continuously exceeded a given threshold, usually 2.5 mK for Nautilus and 5 mK for Explorer. This cuts only a 1 – 2% of the livetime.

A fifth selection is done observing the time distribution of the candidate events, that shows the presence of bursts of events, having duration between 1 or few days down to few minutes (see fig.4). This behaviour is clearly due to some malfunctioning of the detector, not otherwise characterized. The technique employed is to consider periods of time of different duration (usually 1 day, half day, 1 hour, 10 minutes) spanning continuously the livetime, and to count the number of events in each period. We then veto the periods where the number of events found is much higher than that predicted by a Poisson distribution based on the average rate, usually giving a Poisson probability of 10^{-5} or less. This selection is the one resulting in the larger reduction in the number of events, between 50 and 90 %, while reducing the livetime by 10 – 30%.

A last selection requires an uninterrupted operation for a given period, lasting in most cases at least 10 hours. In some cases, this requirement was relaxed down to 5 or 3 hours, in order not to cut more than 30% of the livetime.

The overall cuts produced by these conditions range between 10% and, in few very noisy periods, 70% of the livetime, and between 96 and 99.8 % of the number of events.

4.2. Event selection - Rejection of false candidates events

The relatively small number of events, together with their large amplitude, allows us to analyze each single event and to select those compatible with the assumption to be produced by a very short excitation, such as we expect to be caused by a nuclearite. Figures 5 and 6 show, for Explorer and Nautilus, what a real delta-like event should look like. In both cases, they are real events, produced by a large cosmic rays shower. Note the different shape of the filtered response in the two detectors: it depends on the details of the transfer functions of the two coupled mechanical oscillators (bar and auxiliary resonator) as described in sect 2.1.

A first selection rejects the events vetoed by a coincidence with signals from the cosmic rays detectors. In order to identify an event as due to a cosmic ray shower, and therefore to exclude it from the possible nuclearite events, we require a large number of particles present in both the particle detectors (over and underneath the bar) and a strict time coincidence (less than 10 ms) between their signals and the bar event. This selection takes out only a few events per year.

For each event, we analyzed both the delta-filtered data and the “raw” data, that is the unfiltered ADC readings.

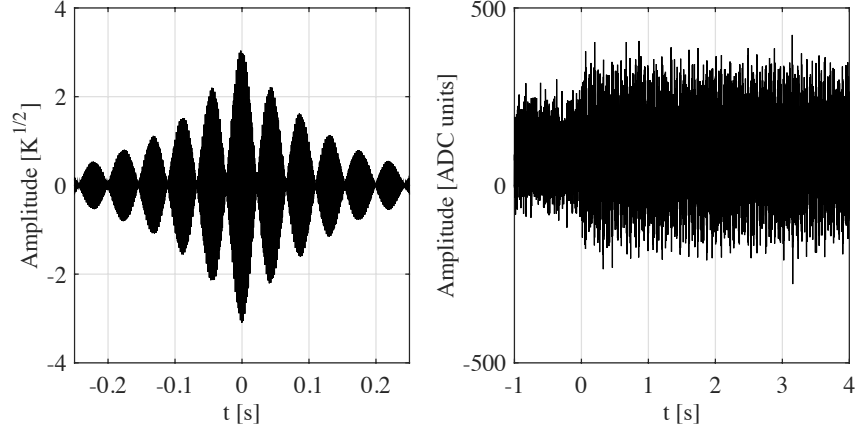


Figure 5: An Explorer event due to a cosmic ray shower: filtered output (left) and raw ADC data (right).

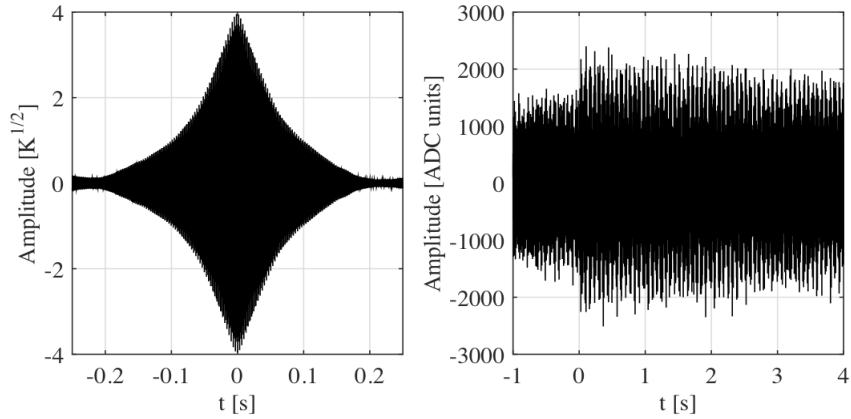


Figure 6: A Nautilus event due to a cosmic ray shower: filtered output (left) and raw ADC data (right).

Examining the filtered data, we reject an event if its shape is judged really incompatible with a delta excitation plus noise. Fig.7 shows some examples of events rejected for this reason.

Candidate events that do appear, after filtering, as delta-like signals, can also be rejected by looking at the direct ADC data: indeed, we saw a large number of strange behaviors that can produce the appearance of a delta-filtered event. There are cases where a very short (few samples) peak appears in the ADC data, most likely due to an electrical spike either in the main power or induced on

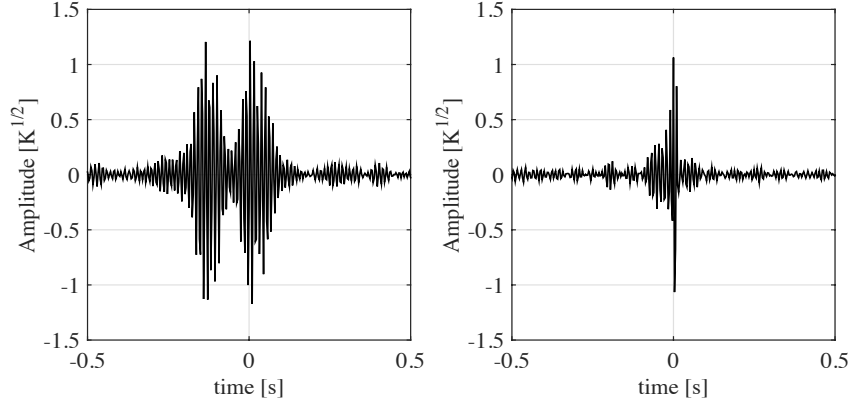


Figure 7: Two examples of filtered events that were rejected due to their shape, bearing no resemblance to the response of Nautilus to a delta signal

the circuitry by some electromagnetic noise (lightnings, for example). In order to quickly identify these instances, we carried out an event search in the ADC data, requiring the presence of a small number of samples above an adaptive threshold.

Then, we perform the coincidence search between these events and the filtered ones, rejecting those in strict coincidence (50 ms).

Another case appears sometimes with the ADC reading dropping to about zero for a few seconds: we know that this happens when the SQUID “unlocks”, i.e. suddenly changes its operating point; indeed we had a veto monitor based on the reading of the SQUID working point, that we used to remove short periods around the times when these jumps occur.

In other cases, but this is apparent only for very large events, we see that the ADC amplitude decays with a time constant much shorter than the one associated with a real mechanical excitation. This happens when an instability causes a resonance in the electrical circuit of the bar transducer. Fig.8 shows examples of this class of rejected events.

Finally, there were few cases when the ADC showed a really erratic or unstable behaviour.

The final result is that these criteria allowed us to reject, as “unacceptable events”, a fraction starting from 7% and up to 93% (depending on detector and period of observation) of the events in the previously defined periods of good operation.

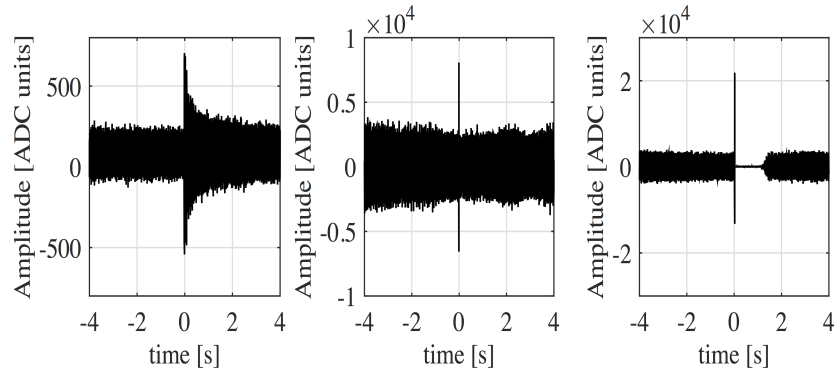


Figure 8: Three examples of events rejected by inspecting the ADC, unfiltered output. From left to right: a decay too short in Explorer (left), a spike lasting few samples, in Nautilus (center), the output going to zero, in Nautilus (right)

4.3. Results on the rate of events

For this work, we have considered the Nautilus data from 2005 to 2014 and the Explorer data from 2005 to the end of its operations, in June 2010. Tab.1 summarizes the results of the present analysis.

As mentioned in sect.4.1, the Explorer data were in general of poorer quality than the Nautilus ones: not only the average T_{eff} is higher, but the high amplitudes tail is larger and there are more instabilities and interruptions. This can be easily seen looking at the results shown in Table1 and it is the reason why we consider the two detectors as “different” and decided not to merge their respective results.

Besides, each detector had varying performances over the full periods in analysis, as shown in figs.9 where we plot the cumulative rates of events vs their energy for the two detectors and for the different years of analysis.

4.4. False dismissal and efficiency

In sect.4.2 we explained the procedures used to reject single events considered incompatible with the kind of excitation we are searching. Here we explain how we evaluated the “false dismissal probability” of these methods, that is the probability that we reject a good delta-like event. In order to evaluate this probability, the procedure calls for the following steps:

- randomly choose N time stamps inside the good operation periods and extract from the filtered data a time segment around those times
- inject in those time segments a copy of a real good event (like for example the ones of fig.5 or 6), scaled to a given value of energy, repeating this for different energies

	Explorer			Nautilus		
Year	Livetime (d)	N.ev.	Rate (ev/y)	Livetime (d)	N.ev.	Rate (ev/y)
2005	153.65870	78	185.41	186.6178	84	164.41
2006	126.03640	107	310.08	135.9331	107	287.51
2007	108.28680	57	192.26	152.9947	67	159.95
2008	131.68350	109	302.33	93.0710	79	310.03
2009	100.70430	167	605.70	191.6569	103	196.29
2010	38.18758	110	1052.11	206.9278	100	176.51
2011				287.8376	160	203.03
2012				300.6588	121	146.99
2013				289.9617	110	138.56
2014				283.4931	286	368.48
Tot	658.55728 (1.803 y)	628	348.31 (avg)	2129.1525 (5.829 y)	1217	208.77 (avg)

Table 1: Characteristics of the bulk of data analyzed, with the final livetimes, number of events and rates.

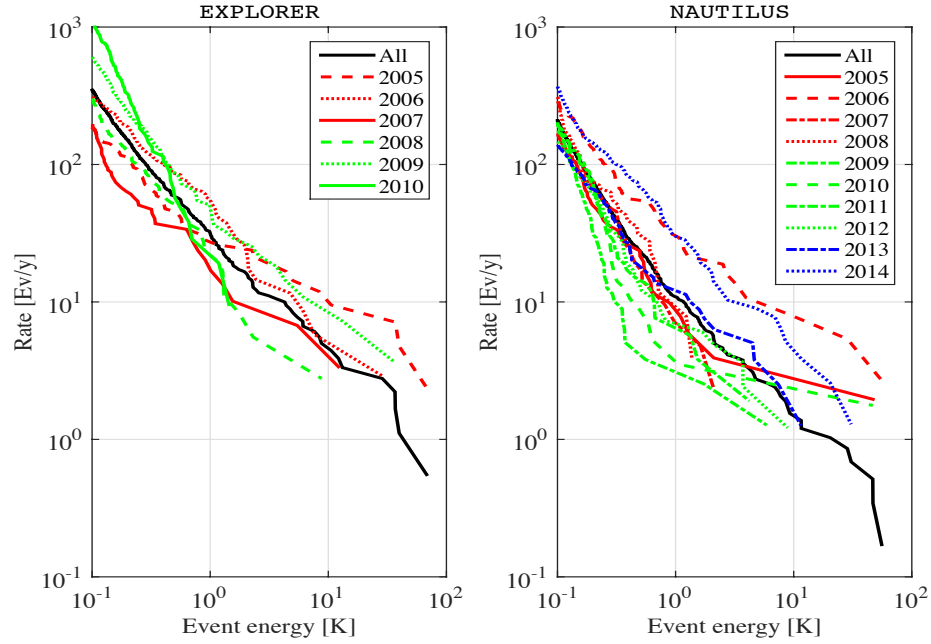


Figure 9: Rate of events of energy larger than the abscissa value for Explorer (left) and Nautilus (right). The different lines are the results at each different year, the overall result is shown with linespoints.

Energy [K]	False dismissal	
	Explorer	Nautilus
0.1	0.08	0.05
0.15	0.01	0.01
0.25	0.01	0.0
0.5	0.0	0.0

Table 2: False dismissal values used in the analysis (see sect. 4.4). They drop to zero, in both detectors, for any signal energy larger than 0.25 K.

- apply to this new time segments (data+event) the selection procedures used to identify bad events and count how many we would reject, at any value of injected energy
- finally, determine the fraction of injected events that were rejected as a function of energy and assume that figure as the probability to reject a real, good event.

The results are summarized in tab.2 and we notice that the false dismissal starts from 8% at the low energy edge for Explorer (100 injected signals in the 2008 data) and from 5% for Nautilus (200 injected signal in the 2007 and 2014 data). Then the false dismissal probability quickly drops, and is zero at all energies above 0.25 K for both detectors.

We applied a similar procedure (injection of copies of a real event at random times for a number of different energies) also to determine the efficiency of detection. In this case we choose 1000 time segments, excluding the segments where an event over threshold was present. We injected copies of a real event scaled at 15 different energy values, ranging from 10 to 200 mK, and counted how many of these events were detected above the 0.1 mK threshold. The results are shown in fig.10.

5. Results

5.1. Nautilus

The cumulative energy distribution of the Nautilus events surviving the cuts described in the previous section is shown in fig.9 . The total livetime is 2129.1 days. This figure shows that the shape of the distribution changes from one year to another. For example the average value of the event energy is 0.2 ± 0.04 K in our “best” year 2011, and 1.24 ± 0.58 K in our “worst” year 2006. This suggests that the operating conditions were not stationary and that there was some unknown source of noise. A serious effort has been carried out to better understand these possible noise sources not considered in the previous paragraph; in particular we have studied the correlation of the noise events with the meteorological condition. We found a weak correlation with the wind speed

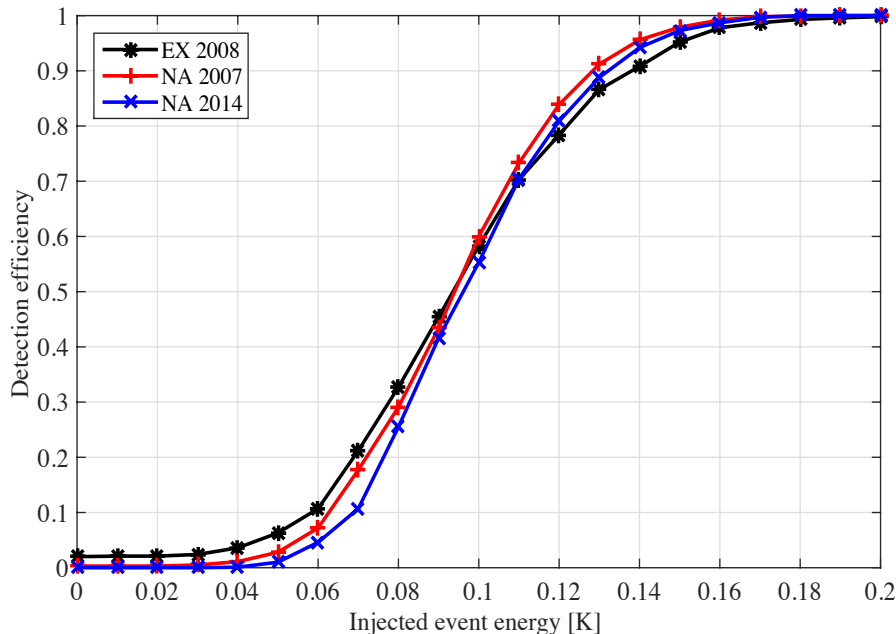


Figure 10: Detection efficiency in three data sets

(or the atmospheric pressure variations). But the correlation is too feeble to proceed to a further data selection.

As an example of the calculations leading to upper limits, we show in Fig.11 the results of Montecarlo simulations for particles of a given mass and velocity: a newtorite of $M/v=10$ kg s/km and a nuclearite of $\beta\theta(M)=0.001$. The two energy distributions are compared with the experimental one.

Note that the energy distribution of the nuclearite shown in this figure is quite different from the data distribution.

For the signal energy distribution we assume that computed by the Montecarlo. Upper limits are computed for different values of $\beta\theta(M)$ and M/v . For both the nuclearite (or Macro) and the newtorite cases, the energy distribution only depends on the geometry, and it is well predicted.

To compute the limits on the maximum allowed number of events for both nuclearites and newtorites, we have used the so called *optimum interval method* to find an upper limit for a one-dimensionally distributed signal in the presence of an unknown background [36, 37, 38].

Tab.3 shows the Nautilus 2005-2014 90% C.L. upper limits on the number of possible nuclearites in the data set, and the resulting limit on the flux. The limits are for an isotropic flux, not considering possible absorption effects by the Earth or the atmosphere (see below). The efficiency is defined as the ratio between the number of events detected with the analysis cuts and the number

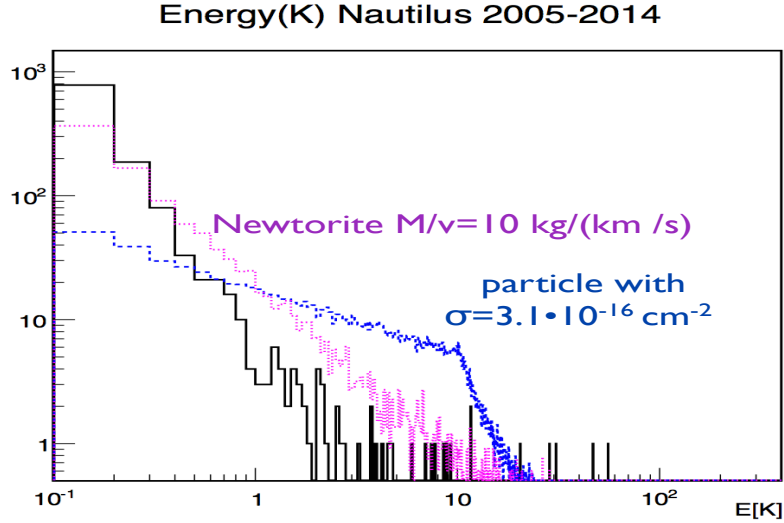


Figure 11: Nautilus 2005-2014 events energy distribution (continuous line) compared with the nuclearite Montecarlo with $\beta\theta(M)=0.001$ (dashed, blue online) and with the newtorite Montecarlo for $M/v=10$ kg s/km (dots, magenta online). For different values of M/v , eq.(11) shows that the mode energy scales with $(M/v)^2$ Montecarlo events are normalized in order to have the same number of events as the real data.

of events hitting the bar.

Tab.4 show the same kind of limits but for Nautilus 2011 only, the year with the lowest noise. The flux upper limits are better than those of the complete data set when dominated by the noise, and are worse at $\beta\theta(M) \gtrsim 0.001$ when they are dominated by the statistics.

Finally, the same upper limits calculation is applied to the case of newtorites, comparing the energy distribution of data and the newtorites Montecarlo. In this case the energy distributions do not change much with the parameter M/v : this is because, as M/v increases, the sensitive volume also increases, allowing detection of signals from newtorites passing at larger distances from the bar. Therefore the upper limits for the number of events is almost insensitive on M/v . In this Montecarlo, newtorites are extracted on a cylindrical surface much larger than the antenna bar. The dimension of the extraction surface is optimized for different M/v ratios (larger for bigger M/v). The Montecarlo therefore computes the efficiency in the case of simulated events that release at least 0.1 K and survive the analysis cuts. For example, the acceptance for the simulation of newtorites of $M/v=10$ kg s/km is $426 \text{ m}^2 \text{ sr}$ (including the efficiencies due to the data selection), while for $M/v=60$ kg s/km the acceptance grows to $2398 \text{ m}^2 \text{ sr}$. The signal energy increases as $(M/v)^2$, this produces a linear increase of the acceptance with M/v .

The results are shown in Tab.5. For sake of uniformity, we have computed the newtorites upper limits using the same optimal interval method as in the nuclearite case. But in this case this tool does not help very much since the

$\beta\theta(M)$	efficiency	σ (cm^2)	events upper limit	flux upper limit ($cm^{-2}s^{-1}sr^{-1}$)
0.0003	0.086	$3.1 \cdot 10^{-16}$	825	$2.7 \cdot 10^{-10}$
0.0004	0.43	$3.1 \cdot 10^{-16}$	727	$4.7 \cdot 10^{-11}$
0.0005	0.61	$3.1 \cdot 10^{-16}$	321	$1.4 \cdot 10^{-11}$
0.0008	0.81	$3.1 \cdot 10^{-16}$	74	$2.6 \cdot 10^{-12}$
0.001	0.83	$3.1 \cdot 10^{-16}$	52	$1.7 \cdot 10^{-12}$
0.002	0.92	$1.25 \cdot 10^{-15}$	9.4	$2.9 \cdot 10^{-13}$
0.004	0.96	$5.0 \cdot 10^{-15}$	3.2	$9.4 \cdot 10^{-14}$
0.01	0.97	$3.1 \cdot 10^{-14}$	2.5	$7.2 \cdot 10^{-14}$
0.02	0.99	$1.25 \cdot 10^{-13}$	2.4	$6.8 \cdot 10^{-14}$

Table 3: Maximum number of nuclearites (or MACRO) events, compatible with the Nautilus energy distribution. Here, and in all following tables, the Upper Limits are calculated at the 90% Confidence Level (C.L.). These values are computed using the optimal interval method. The livetime is 2129.1 days. In the case of nuclearite or of a generic MACRO the shape of the energy distribution depends only on the geometry. The efficiency is defined as the ratio between the number of events detected with the analysis cuts and the number of events hitting the bar. The corresponding cross section σ is for a typical DM velocity $\beta = 0.001$. The flux is considered isotropic when computing upper limits.

shape of the expected energy distribution closely resembles that of the data. As a consequence, it is more important to select data with very low noise than to increase the livetime. In Tab. 6 we can see that the limits obtained using the Nautilus 2011 data are better than those obtained using the full Nautilus data set in almost the entire M/v range.

5.2. Explorer

The Explorer data are selected according to a procedure similar to that of Nautilus. The energy distribution of the events in Explorer, starting from 2005, is shown in fig.9. The total livetime is 658.56 days, much shorter than for Nautilus, also because it ceased operation in June 2010. This figure shows that the shape of the distribution changes from year to year, similarly to what occurs in Nautilus. The corresponding nuclearite upper limits are reported in Tab 7. Explorer and Nautilus are very similar detectors, but there are some differences: e.g. in the geographical location, or in the cosmic ray detectors used as veto. So, it could be interesting to separately analyze their limits before combining the data.

5.3. Nautilus+Explorer

Adding the Explorer noisier data to the Nautilus data degrades the upper limit for low values of $\beta\theta(M)$, where the limit is due to the noise. This data combination is only useful at large values of $\beta\theta(M)$. In Tab. 8 we show the limits for this data combination for nuclearites.

$\beta\theta(M)$	efficiency	events upper limit	flux upper limit ($cm^{-2}s^{-1}sr^{-1}$)
0.0003	0.086	150	$3.6 \cdot 10^{-10}$
0.0004	0.43	55.5	$2.7 \cdot 10^{-11}$
0.0005	0.61	14.3	$4.7 \cdot 10^{-12}$
0.0008	0.81	8.54	$2.2 \cdot 10^{-12}$
0.001	0.83	7.97	$2.0 \cdot 10^{-12}$
0.002	0.92	3.30	$7.4 \cdot 10^{-13}$
0.004	0.96	2.62	$5.6 \cdot 10^{-13}$
0.01	0.97	2.40	$5.1 \cdot 10^{-13}$
0.02	0.99	2.35	$4.9 \cdot 10^{-13}$

Table 4: Nuclearites upper limits as in Tab.3 but for Nautilus 2011, the “best” data set. The livetime is 287.8 days. This data set is the one with the lowest noise. The flux upper limits are better than with the full set of data when dominated by the noise, but are worst at $\beta\theta(M) \gtrsim 0.001$ when they are dominated by the statistics

M/v ($kg\ km^{-1}\ s$)	acceptance ($m^2 sr$)	events upper limit	flux upper limit ($cm^{-2}s^{-1}sr^{-1}$)
1	33.4	545	$8.9 \cdot 10^{-12}$
2	85.3	365	$2.4 \cdot 10^{-12}$
5	209	253	$6.5 \cdot 10^{-13}$
10	426	257	$3.5 \cdot 10^{-13}$
20	888	244	$1.5 \cdot 10^{-13}$
40	1652	248	$8.3 \cdot 10^{-14}$
60	2398	242	$5.5 \cdot 10^{-14}$

Table 5: Nautilus 2005-2014, newtorites upper limits. Note the linear increase of the acceptance with M/v .

6. Discussion and dark matter limits

6.1. Nuclearites

The nuclearite flux upper limits are summarized in fig.12. This figure also shows the limits from a short run with Nautilus at $T = 0.14K$, with live-time= 35.1 days. This result is interesting because of the different detection mechanism in the superconducting state. For $\beta\theta(M) > 0.01$, where the background is negligible, the flux upper limit is dominated only by the live-time. Note that in this search the events in coincidence with the cosmic ray shower detector are removed from the Nautilus data. In principle, fast nuclearites could produce light in the Explorer scintillators (due to black body emission[17]), light that could be confused with a cosmic ray event. Therefore we have verified the “shower” signature of all cosmic rays in the Explorer data: they indeed hit all scintillator counters as expected from a big extensive air shower.

In order to compare our results with previous searches, we recall that many techniques have been used to detect nuclearites: damages in plastic materials like CR39, Makrofol or Lexan, light emission in oil or sea water [40], [41], seismic

M/v $kg\ km^{-1}\ s$	events upper limit	flux upper limit ($cm^{-2}s^{-1}sr^{-1}$)
1	37	$4.5 \cdot 10^{-12}$
2	23	$1.1 \cdot 10^{-12}$
5	22	$4.3 \cdot 10^{-13}$
10	22	$2.1 \cdot 10^{-13}$
20	22	$1.0 \cdot 10^{-13}$
40	22	$5.5 \cdot 10^{-14}$
60	21	$3.5 \cdot 10^{-14}$

Table 6: Nautilus 2011. newtorites upper limits. Livetime=278.8 days, 160 events $\geq 0.1K$

$\beta\theta(M)$	efficiency	events upper limit	flux upper limit ($cm^{-2}s^{-1}sr^{-1}$)
0.0003	0.086	498	$5.2 \cdot 10^{-10}$
0.0004	0.43	409	$8.6 \cdot 10^{-11}$
0.0005	0.61	221	$3.2 \cdot 10^{-11}$
0.0008	0.81	61	$6.9 \cdot 10^{-12}$
0.001	0.83	48	$5.2 \cdot 10^{-12}$
0.002	0.92	11.2	$1.1 \cdot 10^{-12}$
0.004	0.96	3.30	$3.1 \cdot 10^{-13}$
0.01	0.97	2.55	$2.4 \cdot 10^{-13}$
0.02	0.99	2.43	$2.2 \cdot 10^{-13}$

Table 7: Nuclearites upper limits as in Tab.3 but for Explorer from 2005 until 2010. The livetime is 658.5 days. The flux upper limits at $\beta\theta(M) \gtrsim 0.004$ are dominated by statistics.

waves induced by big nuclearites. Due to the uncertainties in the conversion of the energy losses in a measurable signal it is important that different techniques are used to detect such exotic particles.

The best limits above sea level are obtained with track etch detectors, but the detection mechanism is more complicated than the “calibrated” calorimetric technique used in this search. The SLIM limit[42] for $\beta = 10^{-3}$ is $1.3 \cdot 10^{-15} cm^{-2}s^{-1}sr^{-1}$. and the OHYA[43] limit is $3.2 \cdot 10^{-16} cm^{-2}s^{-1}sr^{-1}$, both stated with a 90% confidence limit. The limits from track etch in old mica[44] depend on several additional assumptions. In general we observe that there is no quantitative theory describing the track etch mechanism. Track etch detectors have been calibrated with slow charged ions, assuming energy lost by Coulomb elastic collisions. In principle this process is different from the energy loss of eq.3. The extrapolation of those calibrations to neutral massive particles, losing energy by atomic collisions, is not straightforward. The unique feature of our search is the calorimetric technique that directly measures the energy loss, and therefore is less sensitive to uncertainties or hypotheses in the detection mechanism.

Finally figure 13 shows the upper limits vs the nuclearite mass. For mass between $5 \cdot 10^{-14} g$ (threshold due to the atmosphere) and $10^{-4}g$ this limit is

$\beta\theta(M)$	efficiency	σ (cm^2)	events upper limit	flux upper limit ($cm^{-2}s^{-1}sr^{-1}$)
0.0003	0.086	$3.1 \cdot 10^{-16}$	848	$2.1 \cdot 10^{-10}$
0.0004	0.43	$3.1 \cdot 10^{-16}$	1077	$5.3 \cdot 10^{-11}$
0.0005	0.61	$3.1 \cdot 10^{-16}$	511	$1.76 \cdot 10^{-11}$
0.0008	0.81	$3.1 \cdot 10^{-16}$	112	$2.95 \cdot 10^{-12}$
0.001	0.83	$3.1 \cdot 10^{-16}$	84	$2.13 \cdot 10^{-12}$
0.002	0.92	$1.25 \cdot 10^{-15}$	11.2	$2.58 \cdot 10^{-13}$
0.004	0.96	$5 \cdot 10^{-15}$	3.32	$7.37 \cdot 10^{-14}$
0.01	0.97	$3.1 \cdot 10^{-14}$	2.56	$5.58 \cdot 10^{-14}$
0.02	0.99	$1.25 \cdot 10^{-13}$	2.44	$5.23 \cdot 10^{-14}$

Table 8: Nuclearites (or MACROs) 90% C.L. maximum number of events compatible with the energy distribution of the full data set Nautilus+Explorer, computed using the optimal interval method. The livetime is 2787.6 days. All other considerations detailed in table 3 apply here.

significantly smaller than the flux of galactic dark matter for $\beta = 10^{-3}$ and $\rho_{DM} = 0.3 \text{ GeV}/cm^3$. Although the upper limit of fig.(13) is computed for a set velocity, a sample simulation for $M \leq 1.5 \text{ ng}$ shows that the use of a Maxwell-Boltzmann distribution of velocities, centered at $\beta = 10^{-3}$, produces an upper limit consistent (6% larger) with that reported here.

6.2. MACROs

Nuclearites are a particular kind of MACRO with a specific characteristic: it is supposed to have dimension and cross section always larger than $3.1 \cdot 10^{-16} cm^2$ while a generic MACRO can be smaller. This could have some important experimental implications for track etch mica or plastic detectors. As observed in [9], the requirement for an etchable track is for the burrowed hole in the mica sample to be large enough that hydrofluoric acid can penetrate it during the etching process. This is plausible for hole diameters larger than a few tens of nanometers. Even considering that δ rays (secondary electrons of a few keV) could contribute to enlarge the hole, it is worth noting that the calibrations of track etch detectors are done with charged ions and therefore with object of the size of a few tens of nanometers. This consideration does not apply to gw bar detectors that have no such limitation in the object dimensions.

In crossing the atmosphere and the Earth, the deceleration given by eq.(4) sets bounds on the flux of detectable MACROs as a function of $\frac{\sigma}{M}$. For a down-going vertical track the upper limit is $\frac{\sigma}{M} = 5.6 \cdot 10^{-3} cm^2 g^{-1}$. For a vertical up-going MACRO crossing the Earth the limit is $\frac{\sigma}{M} = 7.8 \cdot 10^{-10} cm^2 g^{-1}$. The upper limits on the cross sections shown in Fig 14 have been computed using the same procedure as for nuclearite.

An allowed region for the MACRO dark matter can be obtained in the plane cross section vs. mass, by excluding the region with upper limit on the flux smaller than the dark matter flux following the approach of Ref [16]. Fig.15

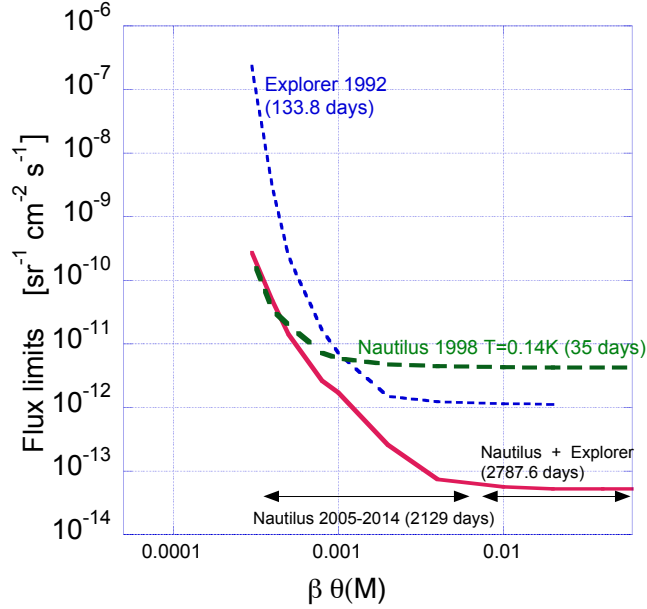


Figure 12: 90% C.L. upper limits for an isotropic flux of nuclearites, compared to previous results (Explorer) [39]. The continuous line shows the results of this analysis. The Explorer data are used in combination to the Nautilus data only for $\beta\theta(M) > 0.002$. For nuclearites that cannot penetrate the Earth, the flux limit should be doubled. Limits from a short run with Nautilus at $T = 0.14\text{K}$, long dashed line, may be interesting because of the different detection mechanism in the superconducting state.

shows the excluded region. It is interesting to observe that studies of cosmological galaxy and cluster halos suggest a value $\sigma/M = 0.1 \text{ cm}^2/\text{g}$ [7, 8]. For the comparison with constraints using other techniques see Ref. [16]. Here, once again, we want to stress the difference of this detector with respect to all other techniques. For small cross sections $\sigma \lesssim 5 \cdot 10^{-17} \text{ cm}^2$ we have a threshold due to the 0.1 K cut used in this analysis. This implies that the excluded area cannot extend below this value. Finally, we remark that for very high cross sections, $\sigma \gtrsim 10^{-14} \text{ cm}^2$, corresponding to signals of the order of $10^4 K$, the efficiency of our search is strongly reduced due to saturation of the data acquisition electronics.

6.3. Newtonites

The limit of Tab. 6 are shown in fig.16 for two values of the velocity $v = 10$ and 300 km/s . We have only used the Nautilus 2011 data set because, in this case, it is more important to have low noise data. The limits reach a plateau as the mass increases. This plateau could in principle extend to very large

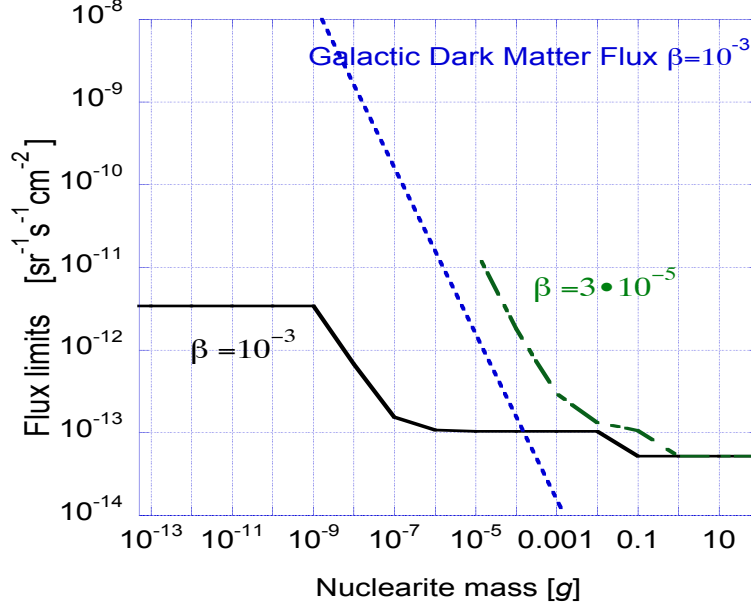


Figure 13: Flux upper limits for nuclearites with $\beta = 10^{-3}$ and $\beta = 3 \cdot 10^{-5}$ (Earth escape velocity) vs mass. The limits are derived from Fig 12, computing the appropriate $\beta\theta(M)$. For some combination of masses and β , nuclearites cannot cross the earth: in this case a factor 2 is applied to the limits of fig.12. For mass between $5 \cdot 10^{-14} g$ (threshold due to the atmosphere) and $10^{-5} g$ this limit is significantly smaller than the flux of galactic dark matter for $\beta = 10^{-3}$.

masses; however, the use of the filter matched to delta - like events limits the search to signals in the ms range and this sets a limitation on d/v where d is the average distance from the bar and v is the particle velocity. In turn, this implies a limitation in the acceptance. Our limit, although very far from the DM expected density ($5 \cdot 10^{-13} kg/km^3$), could be of some interest due to the lack of other experimental limits derived from the direct detection of DM particles that only interact gravitationally and on the Earth.

There are several limits obtained studying the motion of celestial body in the solar system. For example Adler [45] obtains a direct upper limit of the mass of Earth-bound dark matter lying between the radius of the moon orbit and the geodetic satellite orbit. The value obtained is $0.13 kg/km^3$, larger than our limit shown in fig.16. Considering larger volumes Pitjev [46] has found a limit for possible DM inside the Earth-Sun orbits of the order of $1.4 \cdot 10^{-7} kg/km^3$.

Our direct limit on newtorites could be improved by orders of magnitude using two or more nearby bar antennas in coincidence. The performances for newtorites of two antenna in coincidence has been studied by a Montecarlo

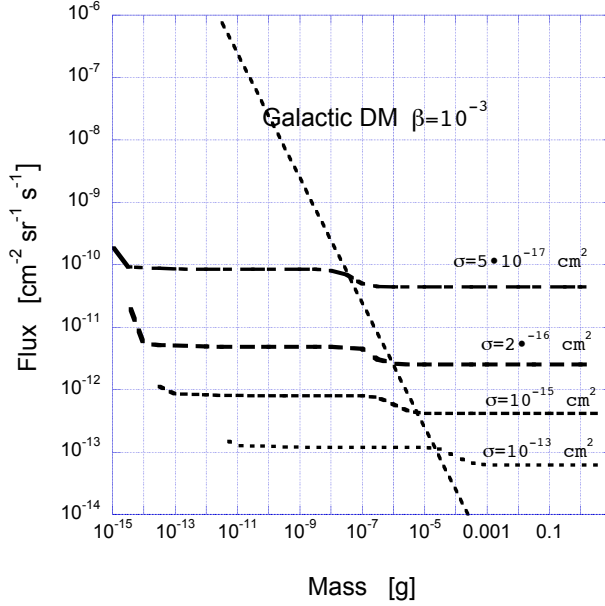


Figure 14: 90 % CL flux upper limits vs MACRO mass for different cross sections. The lowest mass limit on abscissa is set by a mass large enough to cross the atmosphere.

simulation that uses as input the Nautilus 2011 data set (therefore assuming the same performances of Nautilus 2011). In the Montecarlo we assumed two antennas, positioned 1.5 m apart, with uncorrelated noise. Larger distances, up to tens of meters, can still produce a detectable signal, depending on the value of M/v . The result of this study is that a gain of about 300 seems to be possible in 10 years of operations with noise similar to that of Nautilus 2011. This gain is not enough to reach the Pitjev bound. To reach this bound it

is necessary to increase the number of antennas and to reduce their noise. We recall that the current antenna noise is limited by technology and is far from the intrinsic quantum limit of this kind of device $\Delta E = \hbar\omega_0 = 6 \cdot 10^{-31}$ joules. But a large R&D effort would be necessary to approach this limit.

We gladly acknowledge precious help from our technicians M. Iannarelli, E. Turri, F. Campolungo, R. Lenci, R. Simonetti and F. Tabacchioni. We are grateful to our unknown referee, for the careful reading and for many suggestions that prompted us to produce a better paper.

References

- [1] P. A. R. Ade *et al.* [Planck Collaboration], arXiv:1502.01589 [astro-ph.CO].

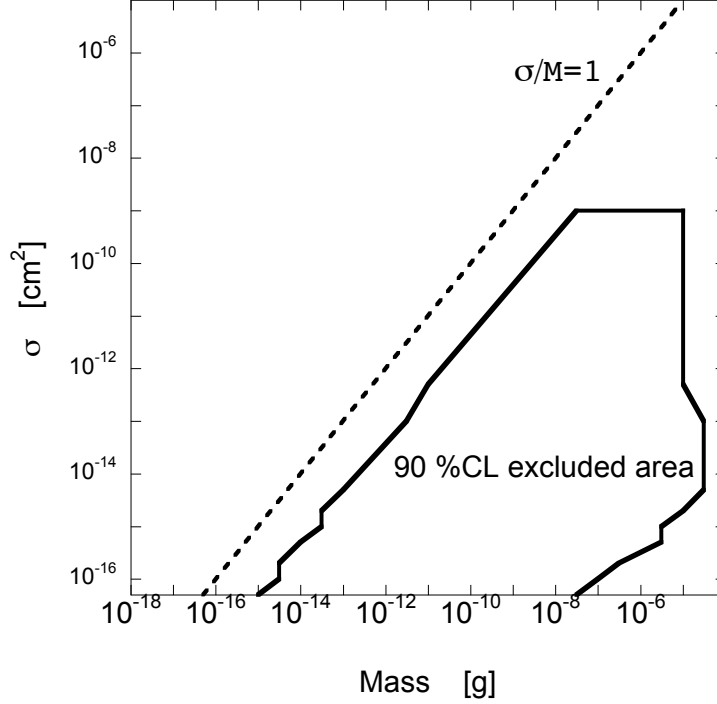


Figure 15: MACRO's 90 % CL excluded regions in the plane cross section - mass. The line $\sigma/M=1$ is drawn for reference. The study of cosmological halos may suggest a value $\sigma/M=0.1$.

- [2] K. A. Olive *et al.* [Particle Data Group Collaboration], Chin. Phys. C **38**, 090001 (2014).
- [3] D. S. Akerib *et al.* [LUX Collaboration], Phys. Rev. Lett. **112**, 091303 (2014) [arXiv:1310.8214 [astro-ph.CO]].
- [4] R. Bernabei, P. Belli, F. Cappella, V. Caracciolo, S. Castellano, R. Cerulli, C. J. Dai and A. d'Angelo *et al.*, Eur. Phys. J. C **73**, no. 12, 2648 (2013) [arXiv:1308.5109 [astro-ph.GA]].
- [5] J. Abraham *et al.* [Pierre Auger Collaboration], Phys. Rev. Lett. **101**, 061101 (2008) [arXiv:0806.4302 [astro-ph]].
- [6] G. Bertone, D. Hooper and J. Silk, 2005 Phys. Rept. 405 279 [hep-ph/0404175].
- [7] M. Rocha, A. H. G. Peter, J. S. Bullock, M. Kaplinghat, S. Garrison-

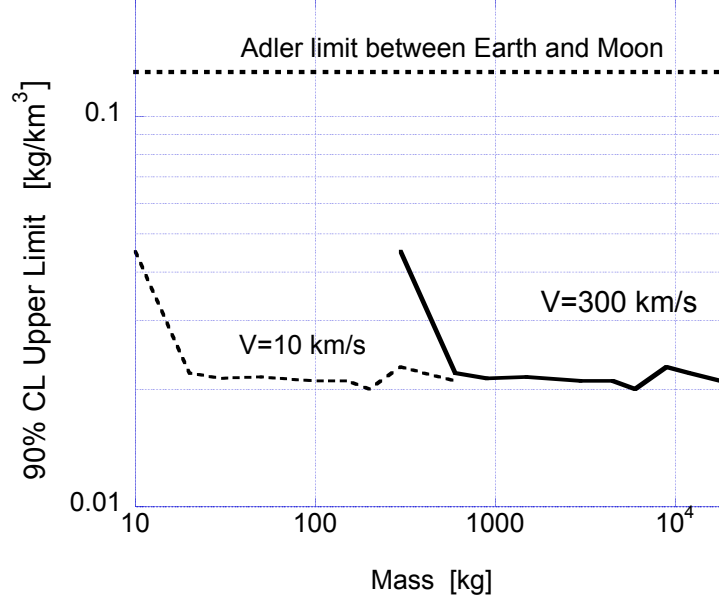


Figure 16: Newtorites density upper limits for $v=10$ and $v=300$ km/s vs the newtorite mass. The limits are obtained from the Nautilus 2011 data set. As the mass increases the limit reaches a plateau

- Kimmel, J. Onorbe and L. A. Moustakas, Mon. Not. Roy. Astron. Soc. **430**, 81 (2013) [arXiv:1208.3025 [astro-ph.CO]].
- [8] A. H. G. Peter, M. Rocha, J. S. Bullock and M. Kaplinghat, Mon. Not. Roy. Astron. Soc. **430**, 105 (2013) [arXiv:1208.3026 [astro-ph.CO]].
- [9] D. M. Jacobs, G. D. Starkman and B. W. Lynn, Phys. Rev. D **91**, 115023 (2015) [arXiv:1410.2236 [astro-ph.CO]].
- [10] Burdin et al. Physics Reports, Volume 582, p. 1-52 (2014) arXiv:1410.1374 [hep-ph].
- [11] G. D. Mack, J. F. Beacom and G. Bertone, Phys. Rev. D **76**, 043523 (2007) [arXiv:0705.4298 [astro-ph]].
- [12] P. W. Gorham, Phys. Rev. D **86**, (2012) 123005/1-8.
- [13] K. Lawson, Phys. Rev. D **83** (2011) 103520/1-9.
- [14] M. Bertaina, A. Cellino and F. Ronga Exp Astron, (2014) DOI 10.1007/s10686-014-9375

- [15] J. Rafelski, L. Labun and J. Birrell, Phys. Rev. Lett. **110**, no. 11, 111102 (2013) [arXiv:1104.4572 [astro-ph.EP]].
- [16] D. M. Jacobs, G. D. Starkman and A. Weltman, Phys. Rev. D **91**, 115023 (2015) arXiv:1504.02779 [astro-ph.CO].
- [17] A. De Rujula and S. L. Glashow, Nature, 312, (1984) 734-737.
- [18] E. Witten, Phys. Rev. D **30** (1984) 272-285.
- [19] A. Dar , A. De Rujula and U. W. Heinz, 1999 Phys. Lett. B 470 142
- [20] J. P. Blaizot, J. Iliopoulos, J. Madsen, G. G. Ross, P. Sonderegger, H. J. Specht, CERN-2003-0001 (2003).
- [21] P. Astone *et al.*, Proceedings of the 33rd International Cosmic Ray Conference, Rio De Janeiro 2013 arXiv:1306.5164 [astro-ph.HE].
- [22] P. Astone *et al.* *Astropart. Phys.* 7 (1997) 231.
- [23] P. Astone *et al.*, Phys. Rev. D 47 (1993) 362.
- [24] M. Bassan *et al.* Nucl. Instrum. Meth. A 659 (2011) 289.
- [25] A.M. Allega and N. Cabibbo, Lett. Nuovo Cimento 38 (1983) 263.
- [26] C. Bernard, A. De Rujula, and B. Lautrup, Nucl. Phys. B 242 (1984) 93.
- [27] G. Liu and B. Barish, Phys. Rev. Lett. 61 (1988) 271.
- [28] D.H. Ezrow, N.S. Wall, J. Weber and G.B. Yodh, Phys. Rev. Lett. 24 (1970) 945.
- [29] P. Astone *et al.*, Phys. Lett. B540 (2002) 179.
- [30] P. Astone *et al.*, Phys. Rev. Lett. 84 (2000) 14.
- [31] P. Astone *et al.*, Phys. Lett. B499 (2001) 16.
- [32] P. Astone *et al.*, Astropart. Phys. 30 (2008) 200 [arXiv:0806.1335 [hep-ex]].
- [33] B. Buonomo *et al.*, Astropart. Phys. 24 (2005) 65.
- [34] M. Bassan *et al.*, Europhys. Lett., 76 (2006) 987.
- [35] M. Barucci *et al.*, Phys. Lett. A 373 (2009) 1801 [arXiv:0901.1220 [gr-qc]].
- [36] S. Yellin, Phys. Rev. D **66**, 032005 (2002) [physics/0203002].
- [37] S. Yellin, arXiv:0709.2701 [physics.data-an].
- [38] We have used the software in the web site:
<http://titus.stanford.edu/Upperlimit/>.

- [39] P. Astone *et al.*, Phys. Rev. D 47 (1993) 4770-4773.
- [40] M. Ambrosio *et al.* (MACRO Coll.), Eur. Phys. J. C, 13, (2000) 453-458
- [41] G. E. Pavalas *et al.*(ANTARES Coll.), Proc. 23rd ECRS, Moscow, 543 (2012).
- [42] S. Cecchini *et al.* (SLIM Coll.), Eur. Phys. J. C, 57, (2008) 525-533.
- [43] S. Orito *et al.* Phys. Rev. Lett. 66 (1991) 1951.
- [44] P. B. Price, Phys. Rev. D, 38, (1988) 3813-3814.
- [45] S. L. Adler, J. Phys. A **41**, 412002 (2008) [arXiv:0808.0899 [astro-ph]].
- [46] N. P. Pitjev and E. V. Pitjeva, Astron. Lett. **39**, 141 (2013) [Astron. Zh. **39**, 163 (2013)] [arXiv:1306.5534 [astro-ph.EP]].